Electrocatalytic arsenite oxidation in bicarbonate solutions combined with CO_2 reduction to formate

Wonjung Choi (Methodology) (Validation) (Formal analysis) (Investigation), Minju Kim (Methodology) (Validation) (Formal analysis) (Investigation), Byeong-ju Kim (Formal analysis), Yiseul Park (Resources) (Funding acquisition), Dong Suk Han (Funding acquisition), Michael R. Hoffmann (Resources), Hyunwoong Park (Conceptualization) (Methodology) (Validation) (Formal analysis) (Resources) (Writing - original draft) (Writing - review and editing) (Visualization) (Supervision) (Project administration) (Funding acquisition)

PII: S0926-3373(20)30022-9

DOI: https://doi.org/10.1016/j.apcatb.2020.118607

Reference: APCATB 118607

To appear in: *Applied Catalysis B: Environmental*

Received Date: 3 September 2019

Revised Date: 21 November 2019

Accepted Date: 6 January 2020

Please cite this article as: Choi W, Kim M, Kim B-ju, Park Y, Han DS, Hoffmann MR, Park H, Electrocatalytic arsenite oxidation in bicarbonate solutions combined with CO_2 reduction to formate, *Applied Catalysis B: Environmental* (2020), doi: https://doi.org/10.1016/j.apcatb.2020.118607

Electrocatalytic arsenite oxidation in bicarbonate solutions combined with CO_2 reduction to formate

Wonjung Choi,[1] Minju Kim,[1] Byeong-ju Kim,[1] Yiseul Park,[2] Dong Suk Han,[3] Michael R. Hoffmann,[4] Hyunwoong Park[1,*]

[1]*School of Energy Engineering, Kyungpook National University, Daegu 41566, Korea*

[2]*Department of Chemical Engineering, Pukyong National University, Busan 48547, Korea*

[3]*Center for Advanced Materials (CAM), Qatar University, Doha 2713, Qatar*

[4]*Linde + Robinson Laboratory, California Institute of Technology, Pasadena, CA 91125, U.S.A.*

*To whom correspondence should be addressed (H. Park)

Tel: +82-53-950-8973; E-mail: hwp@knu.ac.kr

Graphical Abstract

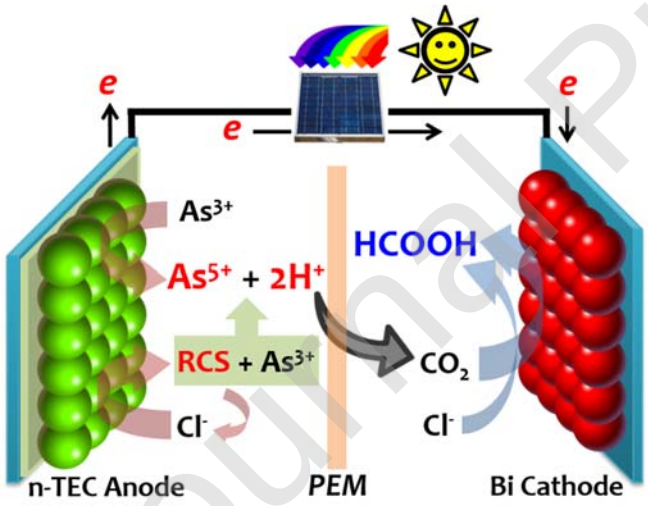

Abstract

Sunlight-driven water-energy nexus technologies are receiving increasing attention. This study presents a hybrid electrochemical system that catalyzes the oxidation of As(III) to As(V) with a nanoparticulate TiO_2 electrocatalyst ($Ti/Ir_{1-x}Ta_xO_y/TiO_2$; denoted as an n-TEC) while simultaneously converting CO_2 to formate on a Bi electrode in aqueous bicarbonate solutions at circum-neutral pH. Linear sweep voltammograms of n-TEC exhibit a specific As(III) oxidation peak ($E_{p,As}$), at which the Faradaic efficiency (FE) of As(V) production is ~100%. However, the application of a potential higher than the peak ($E > E_{p,As}$) leads to a significant decrease in the FE due to water oxidation. Upon the addition of chloride, the oxidation of water and chloride occur competitively, producing reactive chlorine species responsible for mediating the oxidation of As(III). The Bi electrodes synthesized via the electrodeposition of Bi^{3+} typically show high FEs of >80% for formate production in bicarbonate solution purged with CO_2. The addition of chloride significantly enhances the current while maintaining the FE. The n-TEC catalyst and Bi electrodes are paired in a single device equipped with a membrane, and significant effort is made to achieve the same FEs in both the anodic and cathodic reactions as in their half-reactions. Finally, the optimized n-TEC/Bi pair is coupled with a low-cost, commercially available photovoltaic (PV). Various technical factors that drive the overall reactions with the PV are considered, and maximum FEs of ~95% are achieved for the production of both As(V) and formate.

Keywords

Redox reactions; Electrocatalysis; Water treatment; Solar fuels; Water-energy nexus

1. Introduction

Solar CO_2 reduction reactions (CO_2RRs) have received growing attention not only for CO_2 mitigation but also for the production of value-added building-block chemicals [1-3]. There are several types of CO_2 conversion photosystems, including photocatalysis, photoelectrocatalysis, and photovoltaic (PV)-assisted electrocatalysis (**Table S1**). Among them, the last has been considered the most promising due to the easy fabrication, high efficiency, and scalability. Whereas many CO_2 conversion products (C1-C6) are possible, formate is considered one of the most-cost effective (\$0.4 kWh^{-1}), and hence, significant efforts have been made to achieve the selective production of formate at low overpotential and high current [4-9]. Most CO_2RRs have been evaluated in terms of the yield and selectivity of formate [1], particularly in aqueous solutions containing bicarbonate (HCO_3^-), which enhances the CO_2 conversion rate [10,11] and buffering effect, at circum-neutral pH (6.5–8.5). Unfortunately, bicarbonate is not a suitable electrolyte for the oxygen evolution reaction (OER) via water oxidation, which is a counter half-reaction that supplies CO_2 with proton and electron (H^+/e^-) pairs [6,12,13]. It is strongly adsorbed onto the OER electrodes via mono- and bidentate modes [14,15], interfering with the molecular interaction of H_2O with the electrode surface. Furthermore, bicarbonate can be oxidized into carbonate radical anions ($CO_3^{\bullet-}$) by hydroxyl radicals ($OH^{\bullet}$), which are a transient intermediate during the water oxidation, at a relatively high bimolecular rate constant (~10^7 M^{-1} s^{-1}) [16].

Other value-added anodic reactions can be employed as alternatives to the OER to supply CO_2 with H^+/e^- pairs (**Table S1**). One example is the electrocatalytic advanced oxidation reaction of toxic and recalcitrant aquatic substrates via direct and mediated charge

transfer [17-19]. In the former charge transfer, transiently oxidized electrocatalysts withdraw electrons directly from the substrate. In the latter, reactive oxygen and chlorine species (ROS and RCS, respectively) produced via one- or multi-electron oxidations of water (e.g., free $OH^{\bullet}$ and O_3, respectively) [19,20] and two-electron oxidation of chloride ($2Cl^- \rightarrow Cl_2$; $Cl_2 + H_2O \rightarrow HClO + Cl^- + H^+$) mediate the oxidation of the substrate in the bulk solution [21,22]. $OH^{\bullet}$ is preferred to RCS in terms of reactivity [16]; however, its production requires greater energy (2.7 V) than that of RCS (1.3–1.5 V). Coupling of the advanced oxidation reaction with the hydrogen evolution reaction (HER) is well established, as the HER is rather straightforward and proceeds well under various conditions [22-26].

With this in mind, we attempted to simultaneously drive the advanced oxidation reaction and CO_2RR with nearly 100% faradaic efficiencies (FE) for both (**Scheme 1**). To achieve this, Ir and Ta mixed oxides ($Ir_{1-x}Ta_xO_y$) were coated onto Ti foils as an underlayer for an ohmic contact, onto which TiO_2 nanoparticles were coated as an electrocatalytic overlayer [23,27]. As-synthesized nanoparticulate TiO_2 electrocatalysts (denoted as n-TECs) were utilized for the oxidation of As(III) to As(V) in aqueous bicarbonate solutions purged with CO_2 at circum-neutral pH (e.g., $H_3As^{III}O_3 + H_2O \rightarrow H_2As^{V}O_4^- + 2e^- + 3H^+$). Compared to As(III), As(V) is less toxic to humans, while the latter is more removable with conventional techniques (e.g., coagulation, ion exchange, membrane, and adsorption [28-31]. In bicarbonate-free aqueous solutions, As(III) can be oxidized by several ROSs (e.g., $^{\bullet}OH$, $^{\bullet}HO_2/O_2^{\bullet-}$, O_3, and H_2O_2) via advanced oxidation processes [32] including Fenton [33], photolysis [28], and photocatalysis [34]. In the presence of chloride, RCSs can play a primary role in the As(III) oxidation particularly in electrocatalysis [26]. In groundwater with (bi)carbonate, pre-adsorbed As(III) onto metal oxides is released via the formation of arseno-carbonate complexes,

increasing the As(III) concentration in groundwater [35-37]. For the CO_2RR, Bi electrodes were quickly synthesized via the electrodeposition of Bi^{3+} onto Ti foils, and the performance of the Bi electrodes for formate production was optimized. The addition of naturally abundant chloride to the bicarbonate solutions not only mediated the As(III) oxidation via RCS but also enhanced the formate production. Finally, n-TEC and Bi electrode pairs were separated in a two-compartment cell divided by a proton-exchange membrane and coupled with a PV cell to drive the overall redox reactions using sunlight.

2. Experimental section

2.1. Synthesis and characterization of the electrodes

For As(III) oxidation, double-layered electrodes consisting of an $Ir_{1-x}Ta_xO$ underlayer and a nanoparticulate TiO_2 overlayer (denoted as n-TEC) were synthesized following a typical coating-annealing process [21,27,38]. In brief, Ti substrates (Grade 2, ~1 mm thick) were polished with sandpaper and washed with acetone, ethanol, and finally deionized water (>18 MΩ·cm, Human Corporation) in an ultrasonic bath (DAIHAN Scientific Co., Ltd). Then, they were coated with Ir (H_2IrCl_6) and Ta ($TaCl_5$) at a molar ratio of 73/27, followed by annealing at 500 °C for 1 h [38]. The XPS analysis of Ir and Ta for the as-synthesized $Ir_{0.73}Ta_{0.27}O_x$ sample confirmed the composition ratio **(Fig. S1)**. A suspension of TiO_2 nanoparticles synthesized via a typical sol-gel process (Nanopac, Korea) was sprayed onto both sides of the substrates as an overcoat, followed by calcination at 425 °C for 5 h. Our previous studies on the electrodes showed that the underlayer was essential for ohmic contact and durability [17,21,27], and that the TiO_2 overcoat required metal dopants (e.g. Bi and Nb)

[27,39]. However, a further study revealed that the dopant-free TiO_2 electrode exhibited essentially the same performance as the doped one [40].

For the CO_2RR, Bi electrodes were synthesized on the Ti substrates via an electrodeposition process [41]. After drying, the substrates were treated at 500 °C for 6 h in an air atmosphere. The Bi precursor solution was prepared by dissolving bismuth(III) nitrate pentahydrate (50 mM, Junsei) in an aqueous solution containing lactic acid (3 M, Sigma Aldrich, ≥85%) and polyvinylpyrrolidone (5 g L^{-1}, Sigma Aldrich, M.W. 360,000) at pH 3. The electrodeposition was performed in the Bi precursor solution using a typical three-electrode system with the as-prepared Ti substrates as the working electrode, a saturated calomel electrode (SCE) as the reference electrode, and a Pt wire as the counter electrode. A negative potential of −0.847 V vs. SCE was applied to the working electrodes for varying lengths of time (3−60 s). The electrodes were then washed with an ethanol/water mixture and dried [41].

The morphology of the as-synthesized n-TEC and Bi electrodes was examined using a scanning electron microscope (SEM, Su-8230, Hitachi) at an accelerating voltage of 15.0 kV. An energy dispersive spectrometer (EDS, X-MaxN80, Horiba) and an X-ray diffractometer (XRD, Max-2500 V, Rigaku) with Cu Kα radiation (λ =1.5406 Å) were employed to examine elemental composition and crystalline structure, respectively. An n-TEC sample was cut with focused ion beam (FIB, Versa3D LoVac, FEI Company) and its cross-sectional surface was characterized using field-emission electron probe microanalysis (EPMA, JXA-8530F(5CH), JEOL).

2.2. Electrolysis and chemical analysis

The electrochemical behaviors of the n-TEC and Bi electrodes were examined in a customized, single-compartment reactor using a potentiostat/galvanostat (Ivium). Either n-TEC (1 × 1 cm^2 for each side) or Bi electrodes (1 × 1 cm^2; a single side only), and SCE and Pt foil were immersed in aqueous solutions of $KHCO_3$ (0.1 M, Sigma Aldrich, 99.7%) in the absence or presence of CO_2 (99.9999%) purging. The CO_2 purging decreased the electrolyte pH from ~8.5 to ~6.8. For the n-TEC electrodes, the potential was swept from –0.5 to +1.4 V vs. SCE at a rate of 5 $mV \cdot s^{-1}$ in the absence or presence of As(III) (1 mM, $NaAsO_2$, Sigma Aldrich, ≥90%). For the Bi electrodes, the potential was swept from –0.4 to –2.0 V vs. SCE at the same scan rate. If necessary, NaCl or $NaClO_4$ (0.1 M, Sigma-Aldrich, >99.0%) was added to the electrolyte.

The bulk electrolysis for As(III) oxidation using the n-TEC was performed at various potentials (0.75–1.2 V vs. SCE). During electrolysis, aliquots were intermittently sampled and analyzed using the well-known molybdenum blue method for As(V) quantification [26,42]. In brief, aliquots of various volumes (0.1–0.5 mL) were mixed with the molybdate reagent solution (0.2 mL, Sigma-Aldrich) and L-ascorbic acid (0.1 mL, Sigma-Aldrich), and then diluted to a volume of 2 mL using deionized water (18 MΩ cm). After 1 h, the samples were analyzed using a UV-Vis spectrometer (T-60, PG Instruments) at λ = 870 nm. If necessary, As(III) was quantified using high performance liquid chromatography (HPLC, Waters 2695) with an Aminex HPX-87H ion exclusion column (Bio-Rad, 300 × 7.8 mm^2) equipped with a UV detector (λ = 210 nm). 5 mM sulfuric acid was used as an eluent and flowed at 0.6 mL

min^{-1}. The HOCl concentration was estimated using a colorimetric method with UV-Vis spectrometer (UV-2450, SHIMADZU) [21,43].

Formate, which was the primary product of the CO_2RR, was quantified using high performance liquid chromatography (HPLC, Waters Co.) with an Aminex HPX-87H column (BIO-RAD, USA) and a proton nuclear magnetic resonance (H-NMR; Avance III 500 MHz, Bruker) [7,8,44]. If necessary, H_2 in the reactor headspace was analyzed by gas chromatography equipped with thermal conductivity detector (GC-TCD, Agilent 7820). Details of the analytical method can be found elsewhere [6-8]. The concentrations of total chlorine were determined with *N*,*N*-diethyl-*p*-phenylenediamine (DPD) reagent (Hach methods). Hereafter, the unit for electrochemical potential is expressed as V only; "*versus* SCE" is omitted for simplicity, unless otherwise specified.

For As(III) oxidation and simultaneous CO_2RR, a two-compartment Teflon reactor separated by a proton exchange membrane (Nafion 117, Chemours) was designed. n-TEC and Bi electrodes of known area were placed in separate compartments containing 0.1 M $KHCO_3$ in the absence or presence of CO_2 purging. 1 mM As(III) was added to the anolyte. Various DC voltages (E_{DC}) were applied to the n-TEC (anode) and Bi (cathode) pairs, and the current (I_{DC}) was recorded using a DC power supply (E3647A, Keysight Technologies). To estimate the bias potentials at the n-TEC and Bi electrodes at a given E_{DC}, an SCE and Pt wire were placed in either the anode or cathode compartment, and the open circuit potentials of each electrode were measured using a potentiostat (Ivium). If necessary, a known potential was applied to the Bi electrode using the potentiostat. In this case, the n-TEC electrode acted as the counter electrode. For the stand-alone overall processes, a commercial, monocrystalline Si PV cell (Solarcenter Inc.) was connected to the n-TEC and Bi electrode pair and irradiated with simulated sunlight (LS-150-Xe, Abet Technologies, Inc., USA, AM 1.5; 100 $mW \cdot cm^{-2}$). All the electrocatalytic

reactions were performed at least twice.

3. Results and discussion

3.1. Electrocatalytic arsenic oxidation using the n-TEC electrodes.

As-synthesized n-TEC samples were characterized with EPMA (**Fig. 1a** and **b**). The cross-sectional view of the samples obviously shows the sub-micrometer-thick interlayer between the underlying Ti substrate and ~5.5 μm thick TiO_2 overlayer. The interlayer composed of Ir and Ta was uniformly distributed throughout the Ti substrate, whereas our previous attempt led to a localized distribution of Ta [45]. The energy dispersive X-ray spectroscopic analysis of the cross-section further reveals the fractional composition of 87%, 7.6%, and 5.4% for Ti, Ir, and Ta, respectively (**Fig. S2**). The XRD patterns exhibit that TiO_2 was predominant, whereas IrO_2 ($2\theta = 34.46°$ and 58.30° for 101 and 220 planes, respectively) was trace and no Ta-oriented peaks were observed (**Fig. 1c**). Such the weak IrO_2 and absent TaO_x peaks could be attributed to the thick TiO_2 overlayer that inhibits the penetration of the X-ray beam. The primary phase of the TiO_2 overlayer was anatase at ~82% (i.e., rutile of ~18%) [45] due to a relatively low annealing temperature (425 °C) **(Fig. S3)**. The particle size of TiO_2 was ~20 nm (**Fig. S4**), similar to a previous study [45].

Fig. 2a shows the linear sweep voltammograms (LSVs) of n-TEC electrodes in aqueous bicarbonate (BC, 0.1 M) solutions (without or with CO_2 purging) in the absence and presence of As(III) (1 mM). In the pure bicarbonate solution, the onset potential (E_{on}) was ~0.8 V and *I* increased to ~2 mA at E = 1.1 V (*versus* SCE; hereafter omitted for simplicity unless otherwise specified). CO_2 purging did not influence the LSV profile, although the solution pH

decreased slightly from ~8.6 (CO_2-free BC) to ~6.8 (CO_2-purged BC). The addition of As(III) to the CO_2-free bicarbonate solution generated a characteristic peak current ($I_{p,As}$) at ~0.8 V ($E_{p,As}$), followed by a current profile similar to that obtained in the As(III)-free solution. The same magnitude of $I_{p,As}$ with an $E_{p,As}$ shift of ~Δ50 mV was observed when CO_2 was purged into the bicarbonate/As(III) solution. The deviation from *Nernstian* behavior (ΔE = 59 mV/pH ~106 mV) might be attributed to the strong adsorption of carbonic species (HCO_3^- and/or dissolved CO_2) onto the TiO_2 surface and the consequent Fermi level pinning-like effect [46]. This interaction was altered by As(III), as shown by the appearance of $I_{p,As}$ in the presence of As(III). It has been postulated that aqueous As(III) (i.e., $As^{III}(OH)_{3-x}O_x^{x-}$; pK_{a1} = 9.23 [47]) can act as a Lewis base to form the complexes with bicarbonate (e.g., $As(OH)_2CO_3^-$, $As(CO_3)_2^-$, and $As(CO_3)^+$) [35,36,48,49]. Among these, $As(OH)_2CO_3^-$ is considered to be the most abundant at circum-neutral pH (R1) [49,50], and is predominantly adsorbed onto the TiO_2 surface (R2).

$$As(OH)_3 + HCO_3^- \rightarrow As(OH)_2CO_3^- + H_2O,\ K_c = 0.22 \pm 0.04 \quad \text{(R1)}$$

$$>Ti\text{-}OH + As(OH)_2CO_3^- \rightarrow >Ti\text{-}OH\text{--}As(OH)_2 + CO_3^- \quad \text{(R2)}$$

$$>Ti\text{-}OH + As(OH)_3 \rightarrow >Ti\text{-}O\text{--}As(OH)_3^- + H^+ \quad \text{(R3)}$$

where $K_c = [As(OH)_2CO_3^-] / (\gamma_0[As(OH)_3]\times[HCO_3^-])$ and >Ti-OH refers to the TiO_2 surface. In K_c, γ_0 represents the activity coefficient for a neutral species. Assuming $\gamma_0 = 1$, only ~2% of the total As(III) is calculated to exist as complexes (i.e., $[As(OH)_2CO_3^-] \sim 2.2\times10^{-5}$ M), and the free As(III) (i.e., not complexed with carbonic species) can be adsorbed onto the TiO_2 surface (R3). The changes in the LSV induced by the addition of As(III) to aqueous chloride and

perchlorate solutions free of carbonic species (**Fig. S5**) support the direct interaction of the free As(III) with the TiO_2 surface at circum-neutral pH, at which both TiO_2 and As(III) are neutral in charge. The addition of chloride to bicarbonate had an insignificant influence on the LSV profiles (**Fig. 2a**), suggesting that the chloride did not directly affect the As(III)-TiO_2 interaction at $E_{p,As}$.

The bulk electrolysis of As(III) was performed in aqueous bicarbonate solutions in the absence and presence of chloride (see **Fig. S6** for the CO_2-purged condition). As shown in **Fig. 2b**, three bias potentials (E = 0.75, 1.0, and 1.2 V) were selected for the As(III) oxidation ($E°(As^{V}/As^{III})$ = –0.188 V at pH 8.6) [51]. At all three potentials, As(V) was produced linearly for 2 h, and its production accelerated with increasing E (i.e., *I*) (**Fig. 2c**). However, the FE did not exhibit a simple E dependency; the FE was ~100% at E = 0.75 V, and decreased to ~40 and 13% at E = 1.0 and 1.2 V, respectively (**Fig. 2d**). Considering that $E_{p,As}$ is close to 0.75 V (**Fig. 2a**), the ~100% FE value at E = 0.75 V indicates that the direct oxidation of free or complexed As(III) to As(V) occurred efficiently. The FE values at ~100% in different supporting electrolytes further confirm that the direct oxidation of As(III) occurs efficiently as long as the interfacial charge transfer is not altered (**Fig. S7**). The XPS analysis of the n-TEC electrode confirmed the As(III) oxidation to As(V) after 2 h-electrolysis (**Fig. S8**). It is noteworthy that although the fraction of As(V) was only ~20% of a total As (i.e., As(III) = 0.8 mM; As(V) = 0.2 mM), the fraction of As(V) (~55%) on the n-TEC surface was greater than that of As(III) (~45%). This suggests that the adsorption of As(V) is favored over that of As(III). While As(III) oxidation and water oxidation ($E°(O_2/H_2O)$ = 0.48 V at pH 8.6) occur competitively at E = 1.0 V, the latter becomes predominant at E = 1.2 V, significantly decreasing the FE of As(III) oxidation.

The presence of chloride did not influence the As(III) oxidation rate at E = 0.75 and 1.0 V; however, it enhanced the oxidation rate by a factor of two at E = 1.2 V. These changes could be attributed to *I*, which was the nearly same at E = 0.75 and 1.0 V, but increased at E = 1.2 V upon the addition of chloride (**Fig. 2c**). Considering the chlorine evolution reaction (CER, $E°(Cl_2/Cl^-)$ = 1.12 V), the application of E = 0.75 V would be insufficient to directly drive the chloride oxidation. Hence, the FE was nearly the same (~100%) at E = 0.75 V, where the direct As(III) oxidation can occur [51]. This further indicates that the chloride interrupted neither the As(III) adsorption nor the direct charge transfer for the adsorbed As(III). However, a high potential (1.2 V) can oxidize chlorides into RCSs (e.g., $Cl_2^{\bullet-}$ and HClO/ClO^-), effectively mediating As(III) oxidation (R4 and R5).

$$As(OH)_3 + 2Cl_2^{\bullet-} + H_2O \rightarrow H_2AsO_4^- + 4Cl^- + 3H^+ \quad \text{(R4)}$$

$$As(OH)_3 + HOCl \rightarrow H_2AsO_4^- + 2H^+ + Cl^- \quad \text{(R5)}$$

In this case, the pre-adsorption of As(III) is not essential because the RCSs can diffuse into the bulk solution. Such heterogeneous reaction-induced homogeneous bulk reactions are often observed in CER-mediated processes [20,52]. Similarly, other halides (e.g., the I_3^-/I^- couple) have been shown to mediate As(III) oxidation in the bulk [28]. It is noteworthy that although the E° for the CER is ~0.6 V greater than that of the OER at pH ~8.6, the former involving $2e^-$ transfer is kinetically faster than the latter, requiring a lower overpotential [53]. This should lead to a two-fold enhancement of the FE from 13% to 26%. Considering the FE of 30-35% for the CER during electrolysis in the absence of As(III) (**Fig. S9**), ~90% of the produced RCSs (i.e., $FE_{As(V)}$ / FE_{CER}) in the presence of As(III) were estimated to be used to mediate the oxidation of As(III).

To further confirm the RCSs-mediated As(III) oxidation, pre-electrolysis with n-TEC at E = 1.2 V proceeded for 2 h in the absence of As(III) and As(V). Immediately after the electrolysis off, As(III) at 1 mM was spiked to bicarbonate solutions (with and without chloride) and the concentration changes in As(III) and As(V) were examined (**Fig. 3**). As a representative of RCSs, HOCl (i.e., HOCl/OCl^- couple with pK_a of 7.46) was quantified because of the interference effect of bicarbonate on the quantification of total RCSs. In the bicarbonate solution with chloride, the pre-electrolysis led to the gradual production of HOCl to ~0.2 mM in 2 h (**Fig. 3a**). Immediately after the addition of As(III), the concentrations of As(III) and HOCl dropped to ~0.6 mM and zero, respectively, while As(V) at ~0.35 mM was produced (hence total As concentration of ~0.95 mM, nearly matching the spiked As(III) concentration at 1 mM). Considering the equimolar reaction (R5), the larger change in the As(V) concentration than that of HOCl during the post-electrolysis period suggests the involvement of other RCSs (e.g., $Cl_2^{\bullet-}$) in the As(III) oxidation [19-22,24,25,27,52]. The reactivity of RCSs significantly varies depending on the types of the species (e.g., $Cl_2^{\bullet-}$ vs. HOCl) and the substrates (e.g., aliphatic acids vs. aromatics) [21]. If $Cl_2^{\bullet-}$ is predominant, then the oxidation rate can be comparable to that with ROSs (e.g., $OH^{\bullet}$) [19,52]. However, direct comparison of $Cl_2^{\bullet-}$ and $OH^{\bullet}$ for As(III) oxidation in the same electrochemical system is not straightforward, because i) the rate constant with $OH^{\bullet}$ is $>10^9$ M^{-1} s^{-1} [16] whereas that for $Cl_2^{\bullet-}$ is not available in literature, and ii) RCSs are readily produced at high efficiency whereas the production efficiency of ROSs is not high. Particularly in the latter, a chloride electrolyte favors RCSs regardless of the anode material [52], dramatically shifting the reaction mechanism from the ROSs-based to the RCSs-based in most electrochemical systems [19]. In the bicarbonate solution without chloride, the production of neither As(V) nor HOCl was observed and the

spiked As(III) was maintained without any change (**Fig. 3b**).

3.2. Electrocatalytic CO_2 reduction using Bi electrodes

The as-synthesized Bi electrodes fabricated via electrodeposition (ED) were composed of many Bi particle aggregates with a uniform size of ~170 nm (**Fig. 4a** and **b**; see **Fig. S10** for more images). They were homogeneously distributed onto Ti substrate with an overall film thickness of 100-200 nm. The XRD analysis of the sample showed crystalline, rhombohedral structure (JCPDS# 85-1330) with predominant planes of (012), (104), (110), (116), and (214) at 2θ = 27.18°, 38.00°, 39.72°, 62.23° and 70.62°, respectively (**Fig. 4c**). The LSVs of the as-synthesized Bi electrodes always exhibited a cathodic peak at E = –0.84 V in the first potential sweep, which disappeared in the second sweep (**Fig. 4d**). The Bi particles appeared to be partially oxidized while drying in air after ED. In the second cathodic scan, the oxidized species (e.g., BiO_x) should have been reduced to metallic Bi (Bi^0).

The electrocatalytic behavior of the Bi electrodes was compared under N_2 and CO_2 purging (**Fig. 5a**). The E_{on} values were estimated to be −1.6 and −1.4 V, respectively; the difference between them (~0.2 V) was partially attributed to the reduction of the pH from ~9 under N_2 purging to 6.8 under CO_2 purging (ΔE = 59 mV/pH ~0.13 V). It is noteworthy that the *I* under CO_2 purging was significantly greater than that under N_2 purging. This suggests that Bi could effectively catalyze the CO_2RR while inhibiting the HER in bicarbonate solution. To confirm the shift from the HER to the CO_2RR, bulk electrolysis with N_2 purging was performed at E = –1.6 V in a single compartment cell; a stable *I* of ~3.5 $mA \cdot cm^{-2}$ flowed over 2 h with an FE of ~40% for H_2 (**Fig. S11**). On the other hand, under CO_2 purging, a trace of H_2

was evolved (FE < 1%) despite a similar *I* value at the same E (**Fig. S11**); instead, formate was produced linearly with time as the only carbon-containing product with FE of ~80% (**Fig. 5c**). Such the formate production continued over 12 h with the same FE (**Fig. S12**). No other chemicals were found in the gas or liquid phases **(Fig. S13)**; if any were produced, their concentrations were below the detection limit. As the ED time was increased from 3-60 s, E_{on} gradually shifted to positive potential and a larger *I* flowed (**Fig. 5a inset**) due to the greater coverage of the Ti substrate by Bi particles (**Fig. S10**). However, regardless of the ED time, the FE remained nearly the same at 80% (**Fig. 5b**). This suggests that the CO_2RR occurred only on the Bi surface and that the bare Ti surface was inactive for Faradaic charge transfers. In addition, the decreased FE values (60–70%) at low E values (−1.4 and −1.5 V) indicate that a larger overpotential was required for formate production ($E°(CO_2/HCOOH)$ = *ca*. −1 V at pH 6.5). At E = −1.7 and −1.8 V, a larger *I* flowed and consequently, the formate production was enhanced; however, the maximum FE was still ~80% at both potentials. The "magic" FE value of 80% was attributed to the fact that presumably, the produced formate was partially oxidized on the Pt in the single compartment cell. To avoid the possible unwanted reoxidation of formate, the Bi electrode was separated from the Pt counter electrode via a proton-exchange membrane. In this two-compartment cell, a larger amount of formate was produced with an FE of >95% (**Fig. 5c**).

The addition of chloride to the bicarbonate solution further enhanced the electrocatalytic performance of the Bi electrodes; E_{on} was nearly unchanged whereas *I* was significantly improved at E values active for CO_2RR (**Fig. 5a**). In bulk electrolysis at E = −1.6 V, the *I* was approximately two-fold larger, and a proportional increase in the formate production was observed (hence, FE >95%) (**Fig. 5c** and **S14**). It has been postulated that

halides can be specifically adsorbed onto metal cathodes (e.g., Cu and Au) and mediate the charge transfer between the electron-deficient carbon atom of CO_2 (or H^+) and the metal cathodes [54-57]. Such enhanced van der Waals interactions usually enhance *I*, changing the product distribution and as a result the FE values. The same effect appeared to play in a role in increasing *I* without altering the product selectivity in this study. Compared to Cl^-, other halides (I^- and Br^-) have been reported to exert greater effects (e.g., $Cl^- < Br^- < I^-$) due to stronger interactions [55]. However, in this study, they were found to have a negative effect on the formate production and FE (**Fig. S15**). Strong interaction between the halides and the metal surface can facilitate charge transfer from the metal to interfacial CO_2; however, at the same time, such strong adsorption can block and poison the active sites for CO_2RR. Chloride appears to have a moderate strength interaction with the Bi surface, efficiently transferring electrons to nearby CO_2 while being readily desorbed from the surface.

3.3. Designing an electrocatalytic device for arsenic oxidation and CO_2 reduction

To drive the arsenic oxidation and CO_2 reduction reactions simultaneously in a single cell, the LSVs of n-TEC and Bi electrodes (as an anode and a cathode, respectively) of various sizes were compared in bicarbonate solutions purged with CO_2 (**Fig. S16**). As the size was increased, more current flowed, and hence, the DC voltage required for cell operation (E_{cell}) was decreased. Based on the optimal anodic and cathodic half-reaction potentials (e.g., E_a ~0.75 V and E_c ~−1.6 V), an E_{cell} greater than 2.35 V_{DC} must be applied to drive both reactions. However, the simple application of this E_{cell} value based on the difference between E_a and E_c did not actually result in the same performance as those of the half-reactions. For example, n-

TEC and Bi pairs with area ratios of 16-64 at E_{cell} = 2.35 V_{DC} led to FEs of 70-90% and 50-70% for the production of As(V) and formate, respectively (**Fig. S17**). This suggested that a more rational design considering factors associated with the cell resistance (e.g., due to the membrane) and the different catalytic activity of the n-TEC and Bi electrodes was required for energy-efficient redox reactions.

After considering the potential drop across the employed membrane (~0.1 V), we focused on achieving a high FE value for As(III) oxidation rather than for CO_2RR, because the FE of the former is highly susceptible to E (**Fig. 2d** *vs*. **5b**). Then, various E_{cell} values (1.5-3.0 V_{DC}) with different electrode area ratios were tested to find the optimal conditions for both the anodic and cathodic reactions (**Fig. S18**). The first optimal condition was an E_{cell} value of 2.5 V_{DC} with an n-TEC/Bi area ratio of 32 (8 cm^2/0.25 cm^2; denoted as EC-I pair), in which E_a and E_c were maintained at +0.88 V and −1.62 V, respectively. The choice of a large n-TEC electrode was attributed to the high FE at low current density (i.e., small bias) for As(III) oxidation compared to the large potential bias of CO_2RR. It is noteworthy that the obtained E_a (0.88 V) was close to $E_{p,As}$ (0.75 V) (**Fig. 2a**), suggesting direct As(III) oxidation was possible. Accordingly, high FEs (~90%) were obtained for the As(III) oxidation as well as the CO_2RR (**Fig. 6a** and **b**). Unfortunately, I_{cell} was small (max. ~1 mA) under these conditions (**Fig. S19**), and the overall redox reaction was slow. To increase the reaction rate, a larger E_{cell} (3 V_{DC}) was applied to an electrode pair (EC-II pair) with an area ratio of 2. At this voltage, with I_{cell} = 4-5 mA (**Fig. S19** an E_a of 1.26 V and E_c of −1.74 V were obtained. As expected from **Fig. 2** and **5**, the FE of formate production was nearly 100%, whereas the As(V) production was poor with an FE of ~10% due to unwanted water oxidation (**Fig. 6a** and **b**). To inhibit the water oxidation and enhance the As(III) oxidation while not affecting the CO_2RR, chloride was added to

bicarbonate in both compartments. Consistent with **Fig. 2** and **5**, the production of both As(V) and formate was enhanced, with the effect being more pronounced for the former. In the presence of chloride, the FE of formate production was nearly the same (~95%), while that of As(V) was doubled (~22%) due to the RCS-mediated As(III) oxidation (R4).

Based on the above experiments, the electrode pair was coupled to PVs to drive the overall reaction for off-grid operation. The LSVs of two anode/cathode pairs (EC-I and EC-II, with area ratios of 32 and 2, respectively) were compared to the *I*-V curves of the PVs (PV-I and PV-II, with power conversion efficiencies of 12.4 and 12.1%, respectively) (**Fig. 6c**). This comparison suggested that the coupling of EC-I and PV-I could drive direct As(III) oxidation and simultaneous CO_2RR at an E_{cell} of 2.43 V and I_{cell} of 1.47 mA with a maximum solar conversion system efficiency of ~9% (= $E_{cell} \times I_{cell} \times 100\%$ / PV area / 100 mW·cm^{-2}). This efficiency is quite comparable to those of PV-electrocatalysis hybrid systems **(Table S1)**. As expected, both As(V) and formate were produced linearly with time, leading to an FE of ~95% for both reactions (**Fig. 6b** and **d**). However, the actual I_{cell} value (0.5-1 mA) was slightly lower than expected during the bulk electrocatalysis due to the inherent electrochemical polarization. To further enhance the formate production, the coupling of EC-II and PV-II was considered (E_{cell} ~2.8 V and I_{cell} of 5.74 mA; solar conversion system efficiency of ~12%). Using this couple, the formate production was significantly enhanced ~4 times while maintaining an FE of ~95%. However, the As(V) production decreased due to the competitive oxidation of water, and hence, its FE was ~10%. This behavior was similar to that observed for the DC-powered systems. When chloride was added to the bicarbonate solutions, E_{cell} decreased by 0.1 V, while I_{cell} increased from 4 to 4.5 mA (**Fig. S20**). As a result, the formate production was slightly enhanced at the same FE of ~95%, while the As(V) production doubled, with an FE of ~22%

due to the RCS-mediated oxidation of As(III).

Conclusions

This study demonstrated an off-grid hybrid electrocatalytic process for simultaneous As(III) oxidation and CO_2 reduction using a nanoparticulate TiO_2 anode and Bi cathode in aqueous bicarbonate solutions. Although the As(III) oxidation required a low potential bias for n-TEC, its Faradaic efficiency depended significantly on the applied potential, with a value of ~100% at $E_{p,As}$ (~0.8 V) followed by a linear decrease with increasing potential. This dependency was attributed to specific interactions and charge transfer between free or complexed As(III) and TiO_2 at $E_{p,As}$. Potentials greater than the $E_{p,As}$ gradually led to water oxidation, decreasing the Faradaic efficiency of As(V) production. However, in the presence of chloride, the chloride oxidation occurs competitively with water oxidation, effectively mediating the As(III) oxidation and enhancing the Faradaic efficiency. On the other hand, the CO_2 reduction reaction on Bi electrode occurred relatively efficiently as long as a sufficiently negative potential (< -1.5 V) was applied, leading to a Faradaic efficiency of >80% for formate production. In this cathodic reaction, chloride favorably enhanced the current and electron transfer to the Lewis-acidic carbon atom of CO_2. Although both the anodic or cathodic half-reaction could be optimized rather easily, driving both reactions in a single device at the same efficiencies as in the half-reactions was not straightforward due to the cell resistance and the different electrocatalytic activity of the anode and cathode. A well-designed device with a suitably matched photovoltaic was demonstrated to achieve both the anodic and cathodic reactions at high Faradaic efficiencies similar to those in the half-reactions. Despite being a

demonstration at the proof-of-concept level, this study should provide valuable information for designing platforms to realize two different redox reactions in a single device coupled with a photovoltaic.

Declaration of interests

The authors declare that they have no known competing financial interests or personal relationships that could have appeared to influence the work reported in this paper.

Author Contribution Statement

W. Choi: Methodology, Validation, Formal analysis, and Investigation

M. Kim: Methodology, Validation, Formal analysis, and Investigation

B.-j. Kim: Formal analysis

Y. Park: Resources, Funding acquisition

D.S. Han: Funding acquisition

M. R. Hoffmann: Resources

H. Park: Conceptualization, Methodology, Validation, Formal analysis, Resources, Writing – Original Draft, Writing – Review & Editing, Visualization, Supervision, Project administration, and Funding acquisition

Acknowledgements

This research was partly supported by the National Research Foundation of Korea

(2019R1A2C2002602, 2018R1A6A1A03024962, and 2019M1A2A2065616). This publication was made possible by a grant from the Qatar National Research Fund under its National Priorities Research Program (NPRP 10-1210-160019).

References

[1] E.L. Clark, J. Resasco, A. Landers, J. Lin, L.-T. Chung, A. Walton, C. Hahn, T.F. Jaramillo, A.T. Bell, Standards and protocols for data acquisition and reporting for studies of the electrochemical reduction of carbon dioxide, ACS Catal. 8 (2018) 6560-6570.
[2] Y. Hori, Electrochemical CO_2 Reduction on Metal Electrodes, in: C.G. Vayenas, R.E. White, M.E. Gamboa-Aldeco (Eds.) Modern Aspects of Electrochemistry, Springer, New York, 2008.
[3] X. Liu, J. Xiao, H. Peng, X. Hong, K. Chan, J.K. Norskov, Understanding trends in electrochemical carbon dioxide reduction rates, Nature Comm. 8 (2017) 15348.
[4] Carbon Dioxide Utilization. Electrochemical Conversion of CO_2 - Opportunities and Challenges, DNV Report, 2011.
[5] S.K. Choi, U. Kang, S. Lee, D.J. Ham, S.M. Ji, H. Park, Sn-coupled p-Si nanowire arrays for solar formate production from CO_2, Adv. Energy Mater. 4 (2014) 1301614.
[6] N.C. Deb Nath, S.Y. Choi, H.W. Jeong, J.-J. Lee, H. Park, Stand-alone photoconversion of carbon dioxide on copper oxide wire arrays powered by tungsten trioxide/dye-sensitized solar cell dual absorbers, Nano Energy 25 (2016) 51-59.
[7] U. Kang, S.K. Choi, D.J. Ham, S.M. Ji, W. Choi, D.S. Han, A. Abdel-Wahabe, H. Park, Photosynthesis of formate from CO_2 and water at 1% energy efficiency via copper iron oxide catalysis, Energ. Environ. Sci. 8 (2015) 2638-2643.
[8] U. Kang, H. Park, A facile synthesis of $CuFeO_2$ and CuO composite photocatalyst films for production of liquid formate from CO_2 and water over a month, J. Mater. Chem. A 5 (2017) 2123-2131.
[9] S. Kim, W.J. Dong, S. Gim, W. Sohn, J.Y. Park, C.J. Yoo, H.W. Jang, J.-L. Lee, Shape-controlled bismuth nanoflakes as highly selective catalysts for electrochemical carbon dioxide reduction to formate, Nano Energy 39 (2017) 44-52.
[10] M. Dunwell, Q. Lu, J.M. Heyes, J. Rosen, J.G. Chen, Y. Yan, F. Jiao, B. Xu, The central role of bicarbonate in the electrochemical reduction of carbon dioxide on gold, J. Am. Chem. Soc. 139 (2017) 3774-3783.
[11] S. Zhu, B. Jiang, W.-B. Cai, M. Shao, Direct observation on reaction intermedates and the role of bicarbonate anions in CO_2 electrochemical reduction reaction on Cu sufaces, J. Am. Chem. Soc. 139 (2017) 15664-15667.
[12] T.H. Jeon, A.D. Bokare, D.S. Han, A. Abdel-Wahab, H. Park, W. Choi, Dual modification of hematite photoanode by Sn-doping and Nb_2O_5 layer for water oxidation, Appl. Catal., B 201 (2017) 591-599.
[13] T.H. Jeon, G.-h. Moon, H. Park, W. Choi, Ultra-efficient and durable photoelectrochemical water oxidation using elaborately designed hematite nanorod arrays, Nano Energy 39 (2017) 211-218.
[14] H. Park, H.-H. Ou, A.J. Colussi, M.R. Hoffmann, Artificial photosynthesis of C1-C3 hydrocarbons from water and CO_2 on titanate nanotubes decorated with nanoparticle elemental copper and CdS quantum dots, J. Phys. Chem. A 119 (2015) 4658-4666.
[15] H. Park, H.-H. Ou, U. Kang, J. Choi, M.R. Hoffmann, Photocatalytic conversion of carbon dioxide to methane on TiO_2/CdS in aqueous isopropanol solution, Catal. Today 266 (2016) 153-159.

[16] G.V. Buxton, C.L. Greenstock, P. Helman, A.B. Ross, Critical review of rate constants for reactions of hydrated electrons, hydrogen atoms and hydroxyl radicals in aqueous solution, J. Phys. Chem. Ref. Data 17 (1988) 513-886.
[17] J. Kim, W.J.K. Choi, J. Choi, M.R. Hoffmann, H. Park, Electrolysis of urea and urine for solar hydrogen, Catal. Today 199 (2013) 2-7.
[18] S.Y. Yang, Y.S. Choo, S. Kim, S.K. Lim, J. Lee, H. Park, Boosting the electrocatalytic activities of SnO_2 electrodes for remediation of aqueous pollutants by doping with various metals, Appl. Catal., B 111 (2012) 317-325.
[19] S.Y. Yang, D. Kim, H. Park, Shift of the reactive species in the Sb SnO_2-electrocatalyzed Inactivation of E-coli and degradation of phenol: effects of nickel doping and electrolytes, Environ. Sci. Technol. 48 (2014) 2877-2884.
[20] S. Kim, S.K. Choi, B.Y. Yoon, S.K. Lim, H. Park, Effects of electrolyte on the electrocatalytic activities of RuO_2/Ti and Sb-SnO_2/Ti anodes for water treatment, Appl. Catal., B 97 (2010) 135-141.
[21] H. Park, C.D. Vecitis, M.R. Hoffmann, Electrochemical water splitting coupled with organic compound oxidation: The role of active chlorine species, J. Phys. Chem. C 113 (2009) 7935-7945.
[22] S. Kim, G. Piao, D.S. Han, H.K. Shon, H. Park, Solar desalination coupled with water remediation and molecular hydrogen production: A novel solar water-energy nexus, Energ. Environ. Sci. 11 (2018) 344-353.
[23] X. Huang, Y. Qu, C.A. Cid, C. Finke, M.R. Hoffmann, K. Lim, S.C. Jiang, Electrochemical disinfection of toilet wastewater using wastewater electrolysis cell, Water Res. 92 (2016) 164-172.
[24] H. Park, C.D. Vecitis, W. Choi, O. Weres, M.R. Hoffmann, Solar-powered production of molecular hydrogen from water, J. Phys. Chem. C 112 (2008) 885-889.
[25] H. Park, C.D. Vecitis, M.R. Hoffmann, Solar-powered electrochemical oxidation of organic compounds coupled with the cathodic production of molecular hydrogen, J. Phys. Chem. A 112 (2008) 7616-7626.
[26] J. Kim, D. Kwon, K. Kim, M.R. Hoffmann, Electrochemical production of hydrogen coupled with the oxidation of arsenite, Environ. Sci. Technol. 48 (2014) 2059-2066.
[27] H. Park, A. Bak, Y.Y. Ahn, J. Choi, M.R. Hoffmannn, Photoelectrochemical performance of multi-layered BiO_x-TiO_2/Ti electrodes for degradation of phenol and production of molecular hydrogen in water, J. Hazard. Mater. 211 (2012) 47-54.
[28] J. Yeo, W. Choi, Iodide-mediated photooxidation of arsenite under 254 nm irradiation, Environ. Sci. Technol. 43 (2009) 3784-3788.
[29] K. Christen, The arsenic threat worsens, Environ. Sci. Technol. 35 (2001) 286A-291A.
[30] S.Y. Choi, S. Kim, K.J. Lee, J.Y. Kim, D.S. Han, H. Park, Solar hydrogen peroxide production on carbon nanotubes wired to titania nanorod arrays catalyzing As(III) oxidation, Appl. Catal. B 952 (2019) 55-61.
[31] S.I. Siddiqui, S.A. Chaudhry, A review on graphene oxide and its composites preparation and their use for the removal of As^{3+} and As^{5+} from water under the effect of varioius parameters: Application of isother, kinetics and thermodynamics, Process Saf. Environ. 119 (2018) 138-163.
[32] M. Bissen, F.H. Frimmel, Arsenic - a Review. Part II: Oxidation of arsenic and its removal in water treatment, Acta Hydrochim. Hydrobiol. 31 (2003) 97-107.
[33] S.J. Hug, L. Canonica, M. Wegelin, D. Gechter, U. von Gunten, Solar oxidation and removal of arsenic at circumneutral pH in iron containing waters, Environ. Sci. Technol. 35

(2001) 2114-2121.
[34] W. Choi, J. Yeo, J. Ryu, T. Tachikawa, T. Majima, Photocatalytic oxidation mechanism of As(III) on TiO_2: Unique role of As(III) as a charge recombinant species, Environ. Sci. Technol. 44 (2010) 9099-9104.
[35] M.-J. Kim, J. Nriagu, S. Haack, Carbonate ions and arsenic dissolution by groundwater, Environ. Sci. Technol. 34 (2000) 3094-3100.
[36] M. Stachowicz, T. Hiemstra, W.H. Van Riemsdijk, Arsenic-bicarbonate interaction on goethite particles, Environ. Sci. Technol. 41 (2007) 5620-5625.
[37] C.S. Neuberger, G.R. Helz, Arsenic(III) carbonate complexing, Appl. Geochem. 20 (2005) 1218-1225.
[38] O. Weres, Electrode with surface comprising oxides of titanium and bismuth and water purification process using this electrode, US Patent 7,494,583 B2, 2009.
[39] J.M. Kesselman, O. Weres, N.S. Lewis, M.R. Hoffmann, Electrochemical production of hydroxyl radical at polycrystalline Nb-doped TiO_2 electrodes and estimation of the partitioning between hydroxyl radical and direct hole oxidation pathways, J. Phys. Chem. B 101 (1997) 2637-2643.
[40] K. Cho, M.R. Hoffmann, $Bi_xTi_{1-x}O_z$ functionalized heterojunction anode with an enhanced reactive chlorine generation efficiency in dilute aqueous solutions, Chem. Mater. 27 (2015) 2224-2233.
[41] X. Yuan, J. Yi, H. Wang, H. Yu, S. Zhang, F. Peng, New route of fabricating BiOI and Bi_2O_3 supported TiO_2 nanotube arrays via the electrodeposition of bismuth nanoparticles for photocatalytic degradation of acid orange II, Mater. Chem. Phys. 196 (2017) 237-244.
[42] V. Lenoble, V. Deluchat, B. Serpaud, J.C. Bollinger, Arsenic oxidaiton and arsenate determination by the molybdene blue method, Talanta 61 (2003) 267-276.
[43] L.H. Nowell, J. Hoigne, Photolysis of aqueous chlorine at sunlight and ultraviolet wavelengths - I. Degradation rates, Water Res. 26 (1992) 593-598.
[44] U. Kang, S.H. Yoon, D.S. Han, H. Park, Synthesis of aliphatic acids from CO_2 and water at efficiencies close to the photosynthesis limit using mixed copper and iron oxide films, ACS Energy Lett. 4 (2019) 2075-2080.
[45] B.-j. Kim, G. Piao, S. Kim, S.Y. Yang, Y. Park, D.S. Han, H.K. Shon, M.R. Hoffmann, H. Park, High efficiency solar desalination accompanying electrocatalytic conversions of desalted chloride and captured carbond dioxide, ACS Sust. Chem. Eng. 7 (2019) 15320-15328.
[46] H.O. Finklea, Semiconductor Electrodes, Elsevier, Amsterdam, 1988.
[47] G. Liu, X. Zhang, J.W. Talley, C.R. Neal, H. Wang, Effect of NOM on arsenic adsorption by TiO_2 in simulated As(III)-contaminated raw waters, Water Res. 42 (2008) 2309-2319.
[48] Y. Cai, O.C. Braids, Biogeochemistry of Environmentally Important Trace Elements, American Chemical Society2003.
[49] P.A. O'Day, D. Vlassopoulos, X. Meng, L.G. Benning, Advances in Arsenic Research: Integration of Experimental and Observational Studies and Implications for Mitigation, American Chemical Society2005.
[50] C.S. Neuberger, G.R. Helz, Arsenic (III) carbonate complexing, Applied Geochemistry 20 (2005) 1218-1225.
[51] A.J. Bard, R. Parsons, J. Jordan, Standard Potentials in Aqueous Solution, IUPAC, New York, 1985.
[52] Y.Y. Ahn, S.Y. Yang, C. Choi, W. Choi, S. Kim, H. Park, Electrocatalytic activities of Sb-SnO_2 and Bi-TiO_2 anodes for water treatment: Effects of electrocatalyst composition and electrolyte, Catal. Today 282 (2017) 57-64.

[53] K.S. Exner, J. Anton, T. Jacob, H. Over, Controlling selectivity in the chlorine evolution reaction over RuO_2□based catalysts, Angew. Chem. Int. Edit. 53 (2014) 11032-11035.
[54] K. Ogura, J.R. Ferrell III, A.V. Cugini, E.S. Smotkin, M.D. Salazar-Villalpando, CO_2 attraction by specifically adsorbed anions and subsequent accelerated electrochemical reduction, Electrochim. Acta 56 (2010) 381-386.
[55] A.S. Varela, W. Ju, T. Reier, P. Strasser, Tuning the catalytic activity and selectivity of Cu for CO_2 electroreduction in the presence of halides, ACS Catal. 6 (2016) 2136-2144.
[56] R. Pang, X.-G. Zhang, J.-Z. Zhou, D.-Y. Wu, Z.-Q. Tian, SERS chemical enhancement of water molecules from halide ion coadsorption and photoinduced charge transfer on silver electrodes, J. Phys. Chem. C 121 (2017) 10445-10454.
[57] M. Cho, J.T. Song, S. Back, Y. Jung, J. Oh, The role of adsorbed CN and Cl on an Au electrode for electrochemical CO_2 reduction, ACS Catal. 8 (2018) 1178-1185.

Scheme Caption

Scheme 1. Illustration of a PV-coupled electrocatalytic device for As(III) oxidation and CO_2 reduction using an n-TEC anode and Bi cathode, respectively, in aqueous bicarbonate solution (0.1 M) purged with CO_2. n-TEC represents nanoparticulate TiO_2 films deposited on an $Ir_xTa_{1-x}O_y$-coated Ti substrate. In the absence of chloride, the oxidation of As(III) to As(V) and reduction of CO_2 to HCOOH (formate) occurs via a direct charge transfer at high Faradaic efficiencies. In the presence of chloride, transiently formed reactive chlorine species (RCS) mediate the As(III) oxidation while CO_2 reduction is facilitated due to the electron-donating ability of chloride. As^{3+} and As^{5+} represent H_3AsO_3 and $H_2AsO_4^-$ (or $HAsO_4^{2-}$), respectively, at pH ~6.8, while RCS include Cl_2, Cl_2^-, HClO, etc.

Figure Captions

Fig. 1. Surface characterization of as-synthesized n-TEC samples. (a) Cross-sectional EPMA images for Ti, O, Ir, and Ta elements. (b) Depth-profiled elemental distributions of Ti, O, Ir, and Ta. 0 depth refers to the top surface. (c) XRD pattern.

Fig. 2. Electrocatalytic oxidation of As(III) (1 mM) to As(V) using n-TEC electrodes (1×1 cm^2, bifacial) in aqueous potassium bicarbonate (BC) solution (0.1 M) under various conditions. (a) Linear sweep voltammograms (LSVs) in the absence (i.e., BC only) and presence of As(III) (1 mM), Cl^- (0.1 M), and/or CO_2 (purged through the solution). (b-d) Bulk electrolysis of As(III) at various potentials: (b) As(V) production, (c) time-profile current, and (d) Faradaic efficiencies of As(V) production.

Fig. 3. Changes in the concentrations of HOCl, As(III), and As(V) in bicarbonate solutions (a) with and (b) without Cl^- (0.1 M). Prior to spiking As(III) at 1 mM, the solutions underwent pre-electrolysis with n-TEC electrodes at 1.2 V for 2 h. Immediately after the electrolysis off and the addition of As(III), the concentrations of As(III) and As(V) were estimated for the following 1 h. During the pre- and post-electrolysis periods, HOCl was quantified as a representative of RCSs.

Fig. 4. (a) Cross-sectional SEM image of an as-synthesized Bi sample (electrodeposited for 30 s). (b) Particle size distribution of the Bi sample. Inset shows the EDS (left) and top-view SEM image (right). See **Fig. S10** for more images. (c) XRD pattern of the Bi sample. Unassigned peaks refer to Ti substrate. Inset shows the magnified region between 36° and 42° (indicated

with an asterisk), where the Bi peaks (104 and 110) were shown. (d) Linear sweep voltammograms of as-synthesized Bi electrodes (electrodeposited for 30 s) in aqueous bicarbonate solutions (0.1 M) purged with CO_2. The 1st scan represents the voltammogram obtained immediately after synthesis; after the 1st scan, the 2nd potential scan was applied.

Fig. 5. (a) LSVs of Bi electrodes synthesized for 30 s in aqueous bicarbonate (BC) solutions (0.1 M) purged with CO_2 (or N_2 for comparison). If necessary, chloride (0.1 M) was added to the bicarbonate solutions. The inset compares the voltammograms of Bi electrodes in the CO_2-purged bicarbonate solutions as a function of electrodeposition time (0-60 s). (b) Effects of Bi-electrodeposition time (3-60 s) (upper panel) and applied potential (−1.4 to −1.8 V for Bi electrodes synthesized for 30 s) on the Faradaic efficiencies of formate production from CO_2-purged bicarbonate solutions in a single compartment reactor. In the upper panel, an E of −1.6 V was applied for CO_2 reduction. (c) Effect of chloride (0.1 M) on the production of formate and its Faradaic efficiency in CO_2-purged bicarbonate solutions (0.1 M) using Bi electrodes (30 s-sample) at E = −1.6 V in a two-compartment reactor divided by a proton-exchange membrane.

Fig. 6. (a) Electrocatalytic As(III) oxidation and simultaneous formate production using n-TEC and Bi electrodes (EC-I pair with area ratio of 32 at 2.5 V_{DC}; EC-II pair with area ratio of 2 at 3.0 V_{DC}), respectively, placed in a two-compartment cell (divided by a proton-exchange membrane) containing aqueous bicarbonate (0.1 M) solutions purged with CO_2. Note that CO_2 was purged into both the anolyte and catholyte to avoid pH difference between the electrolytes. If necessary, chloride (0.1 M) was added to the both anolyte and catholyte. (b) Faradaic efficiencies (blue and red bars for As(V) and formate, respectively). (c) Comparison of the LSVs of the n-TEC and Bi electrode pairs (area ratios of 32 and 2; denoted as EC-I and EC-II pairs, respectively) and *I*-V curves of the photovoltaics. The specifications of the PVs were as follows: PV-I: Area = 0.4 cm^2, J_{SC} = 6.784 $mA \cdot cm^{-2}$, V_{OC} = 2.64 V, Fill factor: 69.5%, Efficiency = 12.42%. PV-II: Area = 1.32 cm^2, J_{SC} = 4.173 $mA \cdot cm^{-2}$, V_{OC} = 3.65 V, Fill factor: 70.5%, Efficiency = 12.13%. (d) PV-powered simultaneous As(III) oxidation and formate production. With PV-II, chloride (0.1 M) was added to the solution to examine the chloride effect. The other experimental conditions were identical to those of **Fig. 6a**. See **Fig. 6b** for the Faradaic efficiencies.

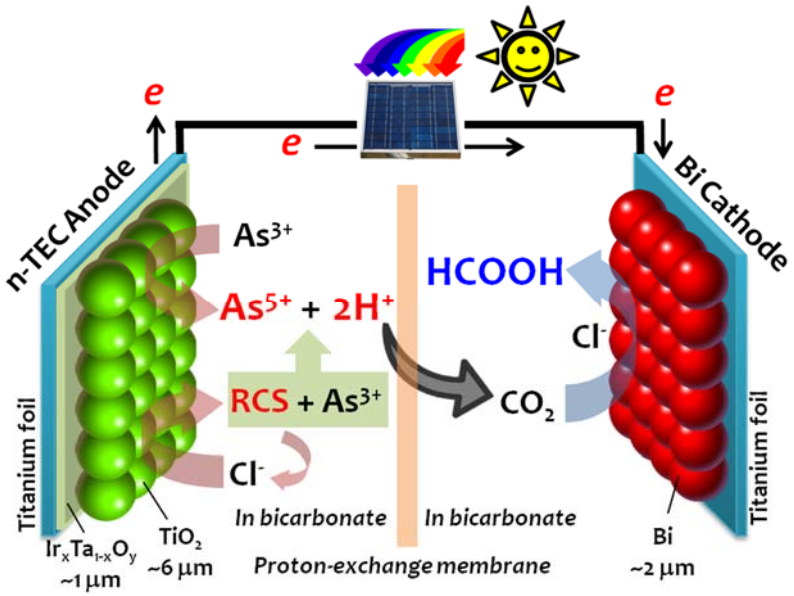

Scheme 1. Illustration of a PV-coupled electrocatalytic device for As(III) oxidation and CO_2 reduction using an n-TEC anode and Bi cathode, respectively, in aqueous bicarbonate solution (0.1 M) purged with CO_2. n-TEC represents nanoparticulate TiO_2 films deposited on an $Ir_xTa_{1-x}O_y$-coated Ti substrate. In the absence of chloride, oxidation of As(III) to As(V) and reduction of CO_2 to HCOOH (formate) occur via direct charge transfer at high Faradaic efficiencies. In the presence of chloride, transiently formed reactive chlorine species (RCS) mediate As(III) oxidation while CO_2 reduction is facilitated by the electron-donating ability of chloride. As^{3+} and As^{5+} represent H_3AsO_3 and $H_2AsO_4^-$ (or $HAsO_4^{2-}$), respectively, at pH ~6.8, while RCS include Cl_2, Cl_2^-, and HClO.

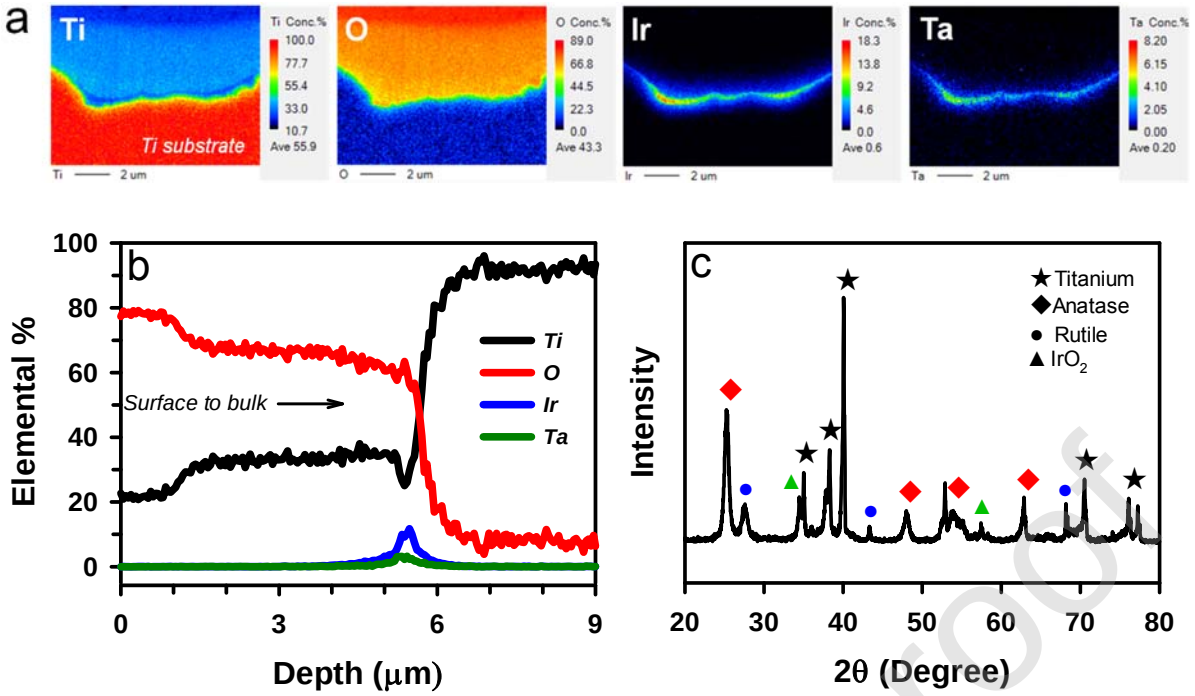

Fig. 1. Surface characterization of as-synthesized n-TEC samples. (a) Cross-sectional EPMA images for Ti, O, Ir, and Ta elements. (b) Depth-profiled elemental distributions of Ti, O, Ir, and Ta. 0 depth refers to the top surface. (c) XRD pattern.

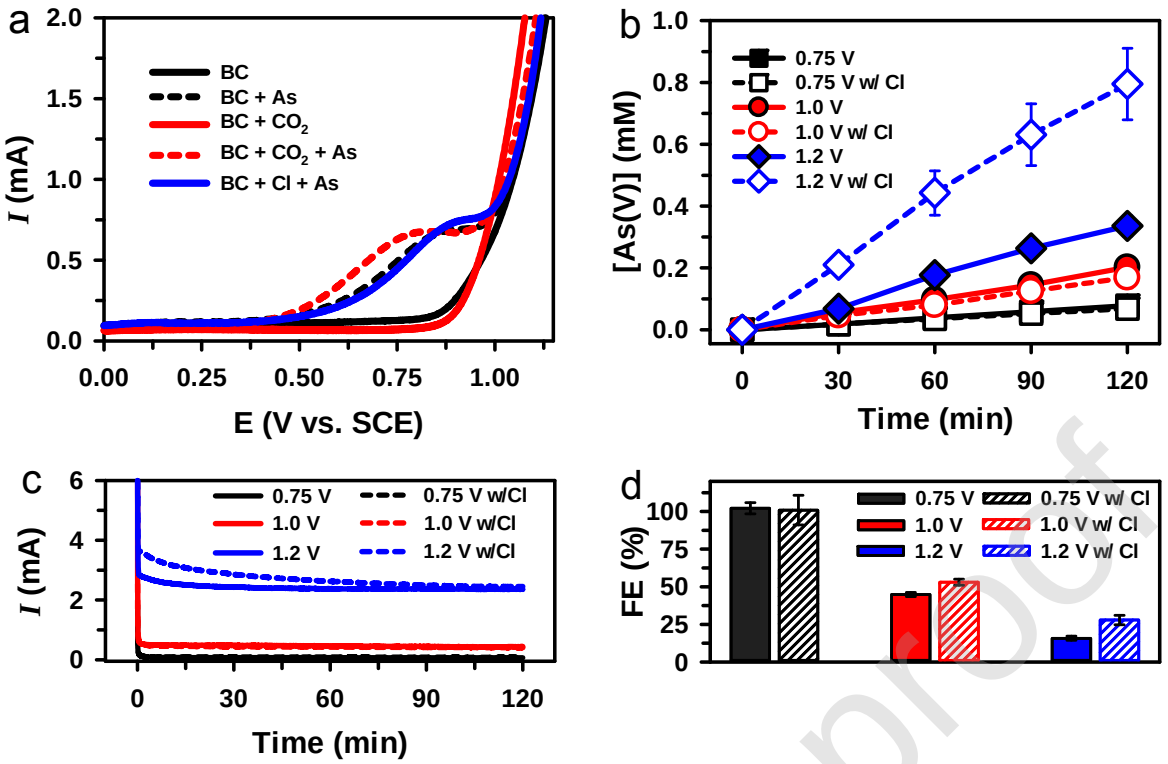

Fig. 2. Electrocatalytic oxidation of As(III) (1 mM) to As(V) using n-TEC electrodes (1×1 cm^2, bifacial) in aqueous potassium bicarbonate (BC) solution (0.1 M) under various conditions. (a) Linear sweep voltammograms (LSVs) in the absence (i.e., BC only) and presence of As(III) (1 mM), Cl^- (0.1 M), and/or CO_2 (purged through the solution). (b-d) Bulk electrolysis of As(III) at various potentials: (b) As(V) production, (c) time-profile current, and (d) Faradaic efficiencies of As(V) production.

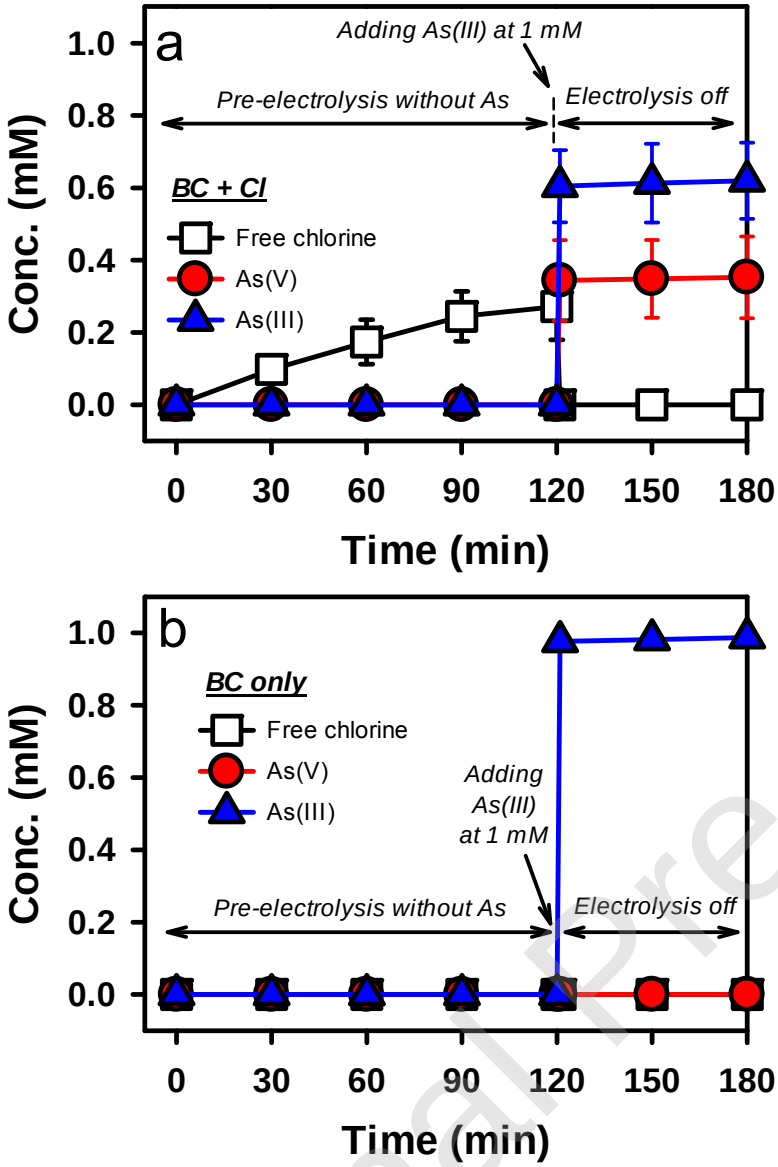

Fig. 3. Changes in concentrations of HOCl, As(III), and As(V) in bicarbonate solutions (a) with and (b) without Cl^- (0.1 M). Prior to spiking As(III) at 1 mM, the solutions underwent pre-electrolysis with n-TEC electrodes at 1.2 V for 2 h. Immediately after the electrolysis and the addition of As(III), the concentrations of As(III) and As(V) were estimated for the following 1 h. During the pre- and post-electrolysis periods, HOCl was quantified as a representative of RCSs.

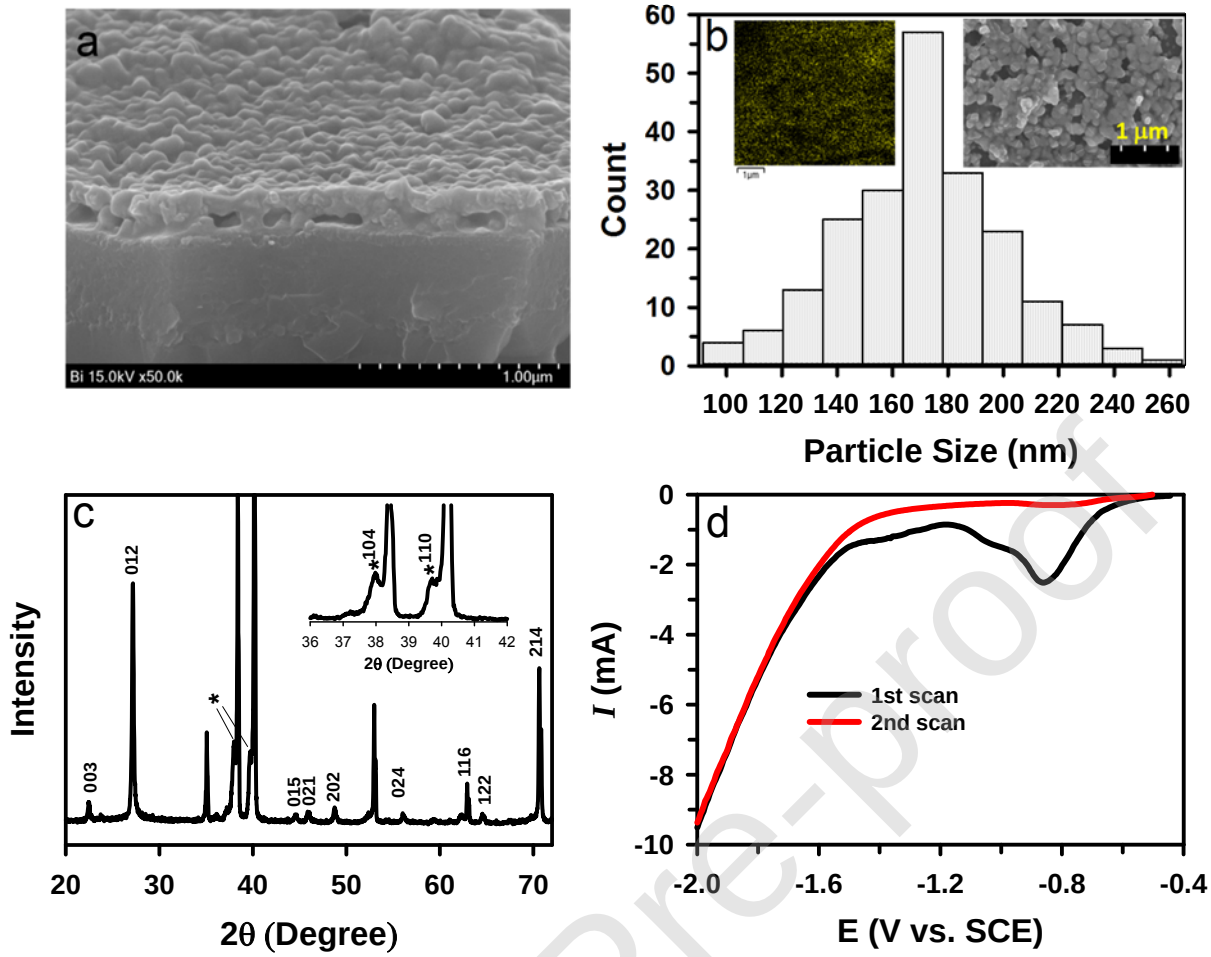

Fig. 4. (a) Cross-sectional SEM image of an as-synthesized Bi sample (electrodeposited for 30 s). (b) Particle size distribution of the Bi sample. Inset shows the EDS (left) and top-view SEM images (right). See **Fig. S10** for more images. (c) XRD pattern of the Bi sample. Unassigned peaks refer to Ti substrate. Inset shows the magnified region between 36° and 42° (indicated with an asterisk), where the Bi peaks (104 and 110) can be seen. (d) Linear sweep voltammograms of as-synthesized Bi electrodes (electrodeposited for 30 s) in aqueous bicarbonate solutions (0.1 M) purged with CO_2. The 1st scan represents the voltammogram obtained immediately after synthesis; after the 1st scan, the 2nd potential scan was applied.

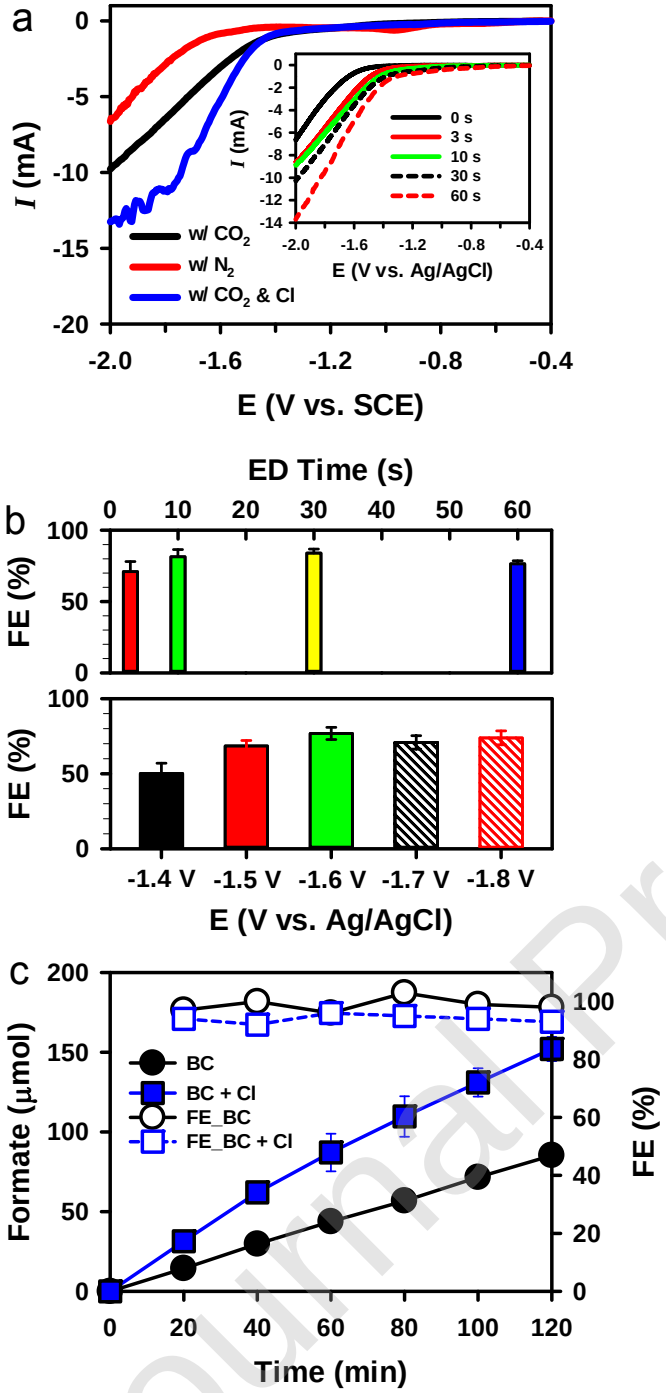

Fig. 5. (a) LSVs of Bi electrodes synthesized for 30 s in aqueous bicarbonate (BC) solutions (0.1 M) purged with CO_2 (or N_2 for comparison). If necessary, chloride (0.1 M) was added to the bicarbonate solutions. The inset compares the voltammograms of Bi electrodes in the CO_2-purged bicarbonate solutions as a function of electrodeposition time (0–60 s). (b) Effects of Bi electrodeposition time (3–60 s) (upper panel) and applied potential (–1.4 to –1.8 V for Bi electrodes synthesized for 30 s) on the Faradaic efficiencies of formate production from CO_2-purged bicarbonate solutions in a single compartment reactor. In the upper panel, an E of –1.6 V was applied for CO_2 reduction. (c) Effect of chloride (0.1 M) on the production of formate

and its Faradaic efficiency in CO_2-purged bicarbonate solutions (0.1 M) using Bi electrodes (30 s sample) at E = −1.6 V in a two-compartment reactor divided by a proton-exchange membrane.

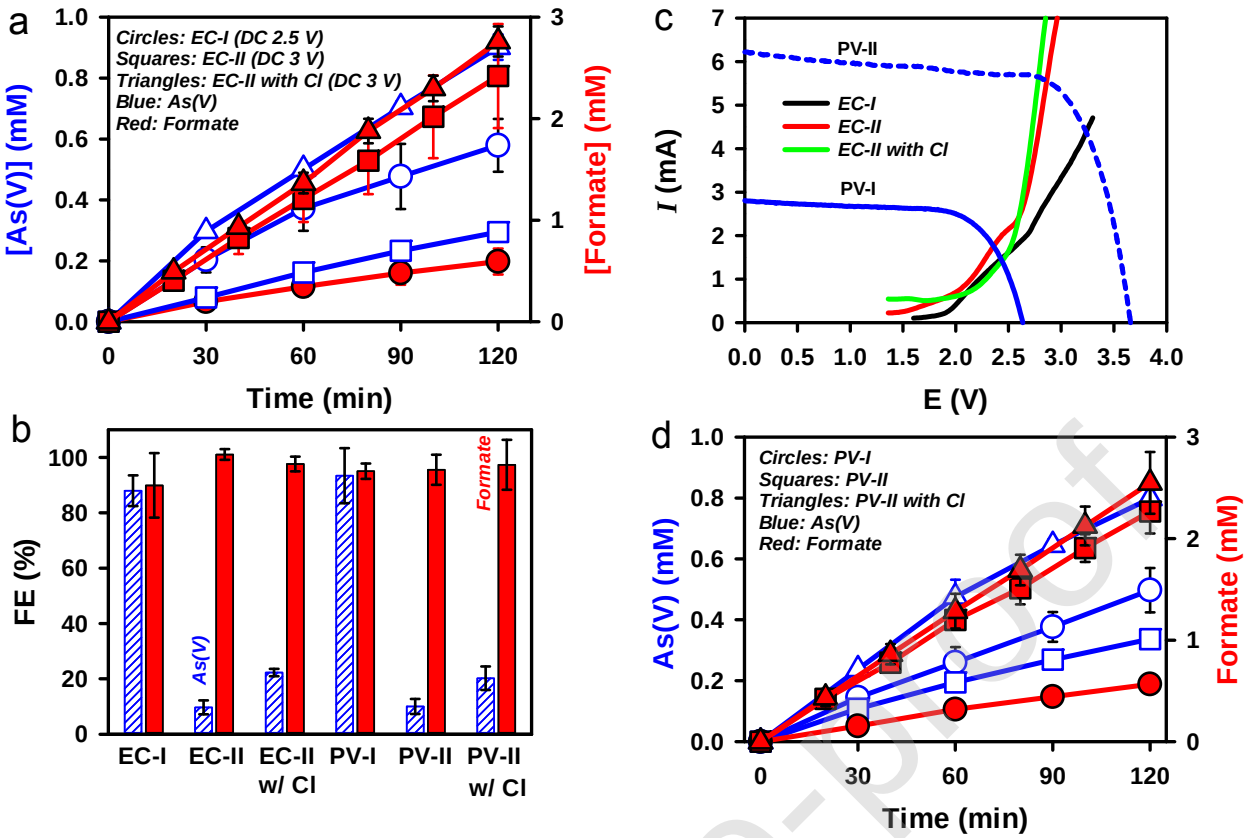

Fig. 6. (a) Electrocatalytic As(III) oxidation and simultaneous formate production using n-TEC and Bi electrodes (EC-I pair with area ratio of 32 at 2.5 V_{DC}; EC-II pair with area ratio of 2 at 3.0 V_{DC}), respectively, placed in a two-compartment cell (divided by a proton-exchange membrane) containing aqueous bicarbonate (0.1 M) solutions purged with CO_2. Note that CO_2 was purged into both the anolyte and catholyte to avoid a pH difference between the electrolytes. If necessary, chloride (0.1 M) was added to both the anolyte and the catholyte. (b) Faradaic efficiencies (blue and red bars for As(V) and formate, respectively). (c) Comparison of LSVs of the n-TEC and Bi electrode pairs (area ratios of 32 and 2; denoted as EC-I and EC-II pairs, respectively) and *I*-V curves of the photovoltaics. The specifications of the PVs were as follows: PV-I: Area = 0.4 cm^2, J_{SC} = 6.784 $mA \cdot cm^{-2}$, V_{OC} = 2.64 V, Fill factor: 69.5%, Efficiency = 12.42%. PV-II: Area = 1.32 cm^2, J_{SC} = 4.173 $mA \cdot cm^{-2}$, V_{OC} = 3.65 V, Fill factor: 70.5%, Efficiency = 12.13%. (d) PV-powered simultaneous As(III) oxidation and formate production. With PV-II, chloride (0.1 M) was added to the solution to examine the chloride effect. The other experimental conditions were identical to those used to obtain results represented in **Fig. 6a**. See **Fig. 6b** for Faradaic efficiencies.